Interdiffusion between silica thin films and soda-lime glass substrate during annealing at high temperature

Jean-Thomas Fonné, Ekaterina Burov, Emmanuelle Gouillart, Sergey Grachev, Hervé Montigaud, Damien Vandembroucq

Interdiffusion between silica thin films and soda-lime glass substrate during annealing at high temperature

Jean-Thomas Fonné, Ekaterina Burov, Emmanuelle Gouillart, Sergey Grachev, Hervé Montigaud

Surface du Verre et Interfaces, UMR 125 CNRS/Saint-Gobain, 93303 Aubervilliers, France

Damien Vandembroucq

Laboratoire PMMH, UMR 7636 CNRS, ESPCI Pariacompanieds, PSL Research University, Sorbonne Université, Université Paris Diderot, 10 rue Vauquelin 75231 Paris cedex 05, France

Abstract

We study the diffusive interaction between soda-lime glass substrates and sputtered aluminum-doped silica thin films at 650°C, the temperature of commercial soda-lime glass shaping or tempering. A first rapid migration of alkali ions from substrate to thin film has been described in a companion paper [1]. Using the same samples as [1], we focus here on later interactions, when the layer is consumed by the substrate resulting from diffusive interactions. Using SIMS profilometry, we show that the interdiffusion rate increases with the aluminum doping content of the layer. We show that the alkali uptake of silica layers accelerates diffusive exchanges with the substrate, consistently with a decrease of viscosity of the layer. Diffusion profiles of silicon are well reproduced when solving the diffusion equation for a diffusivity having an exponential dependence with silicon concentration. The diffusivity of aluminum is shown to be 10 times slower than the diffusion of silicon. Specific exchanges of the two network formers with network modifiers are deduced from the composition-space trajectories, providing evidence for multicomponent diffusive couplings between species.

Keywords: Diffusion/Diffusivity, Silica, Soda-lime glass, Thermal treatment, Thin films, Multicomponent diffusion

1. Introduction

Industrial glasses used in the construction or automotive industry are coated with sputtered thin films. The multilayer stacks of dieletric and metallic films enhance the optical, thermal or mechanical properties of glazings [2, 3, 4]. Coated glasses are often subjected to thermal treatments above the glass transition of the substrate for shaping or tempering purposes. During this annealing stage, alkali species such as sodium or potassium diffuse from the substrate to the coatings, which alters the electrical [5, 6, 7, 8] or mechanical [9, 10, 11] properties of active layers. In order to protect active layers from the migration of alkali, glass substrates are coated with barrier layers such as silica [12, 1], silicon nitride [13] or alumina [14, 15, 5].

In a recent paper [1], we showed that the uptake of sodium by silica barrier layers deposited on soda-lime glass substrates is proportional to the aluminum content of the silica thin film. Aluminum doping is classically used to enhance the deposition rate of silica in industrial Physical Vapor Deposition (PVD) coaters [16]. In addition to the uptake of alkali by thin films, high-temperature treatments also cause interfacial reactions or interdiffusion between substrate and films [17, 18, 19], leading to the consumption of the layer. In this contribution, we pursue our investigations on interactions between glass substrate and silica thin films. We use the same samples described in [1] but focus on later interactions and interdiffusion between film and substrate. More specifically, we study the rate of interdiffusion of aluminum-doped silica layers, resulting from the interdiffusion at high temperature with soda-lime-silica glass substrates used in the building and automotive industry.

The interaction between silica thin films and glass substrates at high temperatures has received little attention in the literature, contrary to other systems such as thermal barrier coatings on metallic alloys [20, 21]. At a larger scale, the contact between silicate liquids or glasses of different compositions has been studied ex-

tensively in the geochemistry community [22, 23, 24]. The relation between viscosity and diffusion of silicon and oxygen has been shown to be well approximated by the Eyring relation at high temperature [25]. In addition, diffusion processes are cooperative because of the strong polymerization of the silicate network. Therefore, a *diffusion matrix* is needed to fully describe multicomponent diffusion exchanges in silicate liquids [26]. The diffusion matrix has been determined for a variety of silicate compositions in ternary diagrams [27, 28, 29, 30, 31], with a few studies in more complicated systems [32, 33, 34].

Here we study the interdiffusion at 650°C between PVD-sputtered Al-doped silica thin films and a soda-lime-silica glass substrate. Using Secondary Ion Mass Spectroscopy (SIMS), we measure the rate of silica layer consumption and the composition profiles of the different chemical species.

In the following we first present the experimental methods used in this study to fabricate and characterize the silica thin films deposited on glass substrate and their evolution upon annealing at high temperature, and we give a focus on the formalism of the multicomponent diffusion. We then present the concentration profiles of the different oxides obtained for increasing annealing time at 650°C and we give evidence of a gradual diffusive consumption process of the silica thin films by the glass substrate. We finally discuss our results along three lines: the counter-intuitive effect of aluminum doping on the diffusivity and viscosity of the silica thin films, related to increased alkali uptake as shown in [1]; the modelling of the diffusive transport of silica and alumina in the presence of a diffusivity gradient; the interpretation of our results in the framework of multicomponent diffusion.

2. Materials and methods

The materials used in this study are the same as in our previous study [1]. However, we reproduce here part of the sample description and analysis methods for the sake of completeness.

2.1. Glass substrates

Commercial Saint-Gobain Planiclear flat glass with a thickness of 2 mm is used as glass substrates. The composition in weight percent (wt%) of this soda-lime float glass is given in Table 1. The atmospheric sides of the Float glass were cleaned with RBS^{TM} and rinsed with deionized (DI) water before thin film deposition.

Table 1: Composition in weight percent (wt%) of the soda-lime glass substrates.

oxides	wt%
SiO_2	73.0
Na_2O	13.5
CaO	10.0
MgO	2.5
Al_2O_3	0.5
K_2O	0.1
Other elements	< 0.4

2.2. Silica thin films deposition

In this study, we consider four types of silica thin films with different alumina doping contents: 0, 0.5, 0.8 and 4.3 wt%. Aluminum doping is indeed used in most industrial PVD coaters in order to accelerate the deposition rate [16], but little knowledge is available about its effect on substrate - layer interaction during annealing.

For the four compositions, thin films were deposited by reactive magnetron sputtering at room temperature. Pure silicon and silicon with 8% in weight of aluminum targets were used for silica thin films deposition, operating in DC mode. The base pressure was 10^{-7} mbar and the operating pressure was monitored at 2 μbar by the flow rate of argon and oxygen and the pumping system. Silica layers containing 0 wt% and 4.3 wt% of Al_2O_3 were obtained by using a single target and SiO_2 thin films with 0.5 and 0.8 wt% of Al_2O_3 were obtained by co-sputtering with the two targets. No bias or additional heating was applied to the substrate during the deposition process.

The thickness of the films was measured with surface profilometry (DektakXT, Brucker) or atomic force microscopy (Icon, Brucker). Silica thin films with thicknesses between 100 to 250 nm were used for this study [1]. Several deposition chambers were used for this work depending on the size of the samples and the configuration needed (sputtering or co-sputtering). Only results for silica layers with thicknesses of 150 or 220 nm are presented in this paper.

2.3. Thermal treatments

After deposition of silica thin films on glass, samples were annealed in air in an electrical furnace at 650°C, a common temperature for glass shaping or tempering. This temperature is above the glass-transition temperature (T_g) of the substrate (~ 550°C) and thus allows migration of network modifiers and formers between glass and silica. Annealing durations between 15 min and 4

hours were performed at this temperature. Samples were directly placed in the furnace pre-heated at 650°C and quenched in air at the end of the thermal treatment.

2.4. ToF-SIMS measurements

SIMS depth profiles of annealed samples were carried out on a TOF.SIMS 5 (IONTOF GmbH, Münster, Germany). Cs^+ was selected as abrasive species since it induces less artefacts than oxygen ions due to alkalis ions migration during depth profiling. The sputter beam energy was 2 keV and the applied current was 150 nA. The analysis beam, operating in pulsed mode for the ToF mass spectrometer, was composed of Bi^+ ions at 30 keV with a current of 3 pA. The scanned area measured 50 x 50 μm^2 in the middle of the abrased zone measuring 200 x 200 μm^2. In order to reduce charging effects, a low-energy electrons flood gun was used.

In Ref. [1], we have described in detail SIMS acquisitions in silica thin films and calibration of SIMS measurements for quantitative values of depth and composition. The interested reader is referred to this publication for details on the method. Briefly, depth is calibrated using stylus profilometry on SIMS craters. Chemical composition is calculated from secondary ions signals by assuming that sensitivity factors for each element are comparable in the substrate (of known composition) and in the layer or interface. These estimations have been verified using XPS and electron microprobe analysis [1].

2.5. Multicomponent diffusion formalism

In this paragraph, we recall the equations used for predicting and fitting chemical concentration profiles resulting from molecular diffusion in silicate liquids.

Chemical diffusion of a single species is described by Fick's first law

$$\mathbf{j} = -D\nabla C, \tag{1}$$

a linear relation between the flux $\mathbf{j}$ and the concentration gradient ∇C. The linear coefficient D is called the diffusion coefficient or diffusivity of the element. In the absence of other fluxes (e.g. due to convection), one obtain the second Fick's law from mass conservation

$$\frac{\partial C}{\partial t} = \nabla \cdot (D\nabla C), \tag{2}$$

also known as diffusion equation. When the diffusivity is constant, the above equation simplifies to

$$\frac{\partial C}{\partial t} = D\nabla^2 C. \tag{3}$$

However, in the case of strong concentration gradients one cannot always assume that diffusivity is constant, so that Eq. (2) has to be solved instead. The boundary conditions are given by the spatial configuration of the materials diffusing together.

In silicate liquids, a complete description of chemical diffusion requires to account for couplings between species. This is done by considering that the flux of one species i depends linearly on the gradients of all present species

$$\mathbf{j}_i(\mathbf{x}) = -\sum_k D_{ik}\nabla C_k(\mathbf{x}), \tag{4}$$

which leads to the multicomponent diffusion equation

$$\frac{\partial C_i}{\partial t} = \sum_k \nabla \cdot \left(D_{ik}\nabla C_k\right), \tag{5}$$

or in vectorial form

$$\frac{\partial \mathbf{C}}{\partial t} = \nabla \cdot (\mathbf{D}\nabla \mathbf{C}), \tag{6}$$

where $\mathbf{C} = (C_1, \ldots, C_n)$ is the vector of local concentrations, and $\mathbf{D}$ is the $n \times n$ diffusion matrix.

The eigenvectors of the matrix $\mathbf{D}$ describe invariant directions in the space of composition gradients, and can therefore be interpreted as elementary exchange reactions between species [35, 34]. The associated eigenvalues are the diffusivity of each exchange reaction.

3. Results

3.1. Chemical evolution of silica layer and interface

SIMS profiles for the major elements of glass substrate and layer are shown in Fig. 1 for different annealing times at 650°C and the two extreme layer compositions that we tested: a pure silica layer and a silica layer doped with 4.3 wt% of alumina. The position of the initial interface is represented with a dotted line.

As reported in Ref. [1], thermal annealing first induces in the thin film a rapid uptake of alkali up to a partial equilibrium concentration that is controlled by the initial alumina content of the deposited layer. After 15 minutes, the sodium concentration is thus almost constant within the thin film but with contrasting values: about 0.2 wt% in the pure silica layer versus 3.8% in the 4.3% doped aluminum layer (see Fig. 1 c) and g)). In Ref. [1], we showed that the partial equilibrium concentration of sodium in an Al-doped silica layer is proportional to the aluminum content, with an empirical relation between molar concentrations:

$$C^{\mathrm{mol}}_{\mathrm{Na_2O}} = 1.47\, C^{\mathrm{mol}}_{\mathrm{Al_2O_3}} + 0.22. \tag{7}$$

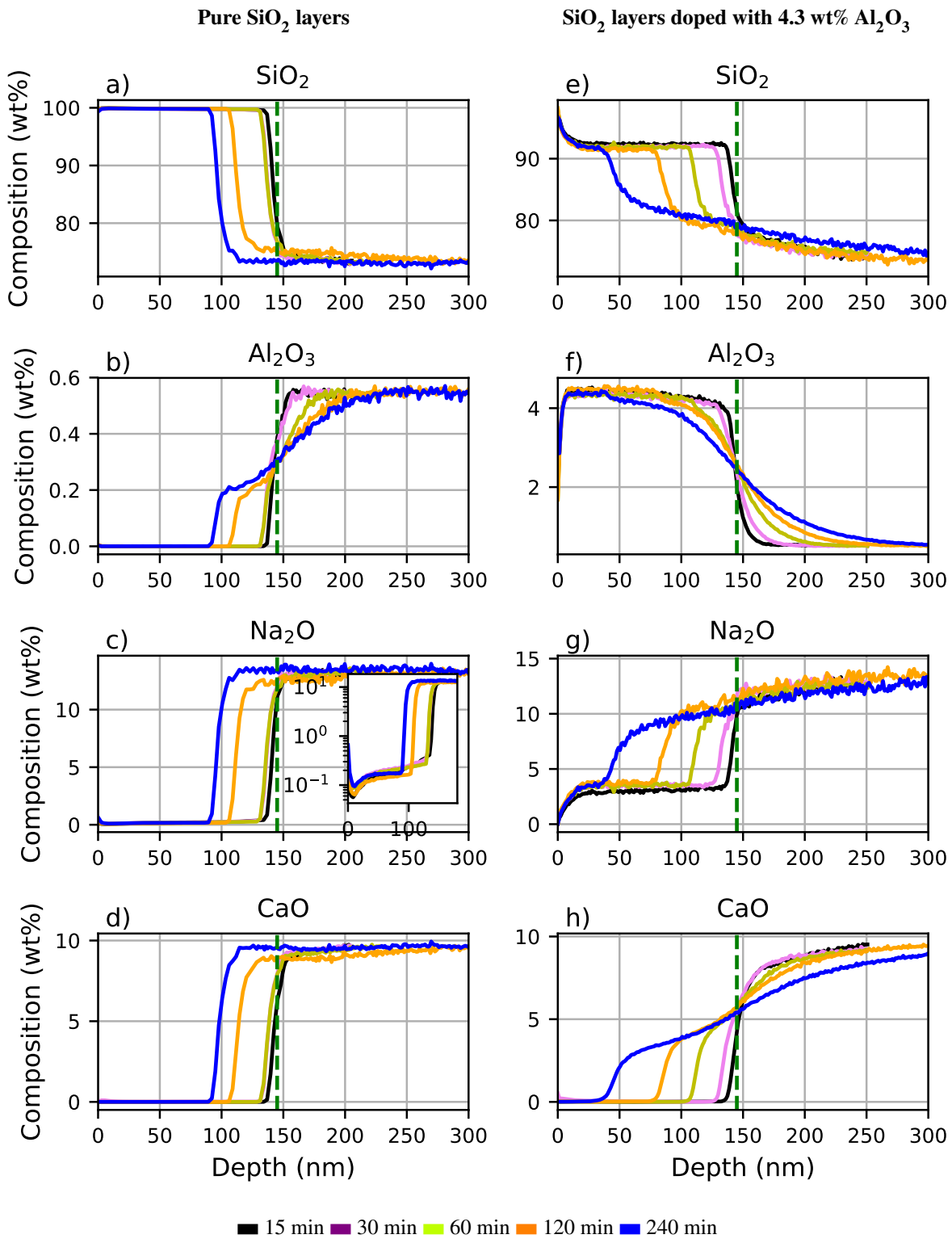

Figure 1: SIMS profiles for different oxides of a 150 nm pure silica thin film (left) and a 4.3 wt.% Al_2O_3-doped silica thin film (right) for various annealing durations at 650°C. Oxides concentrations are given in weight %. The interface before annealing (vertical green dotted line) is followed by the maximal value of the Sn^+ peak during SIMS analysis. In c), a log-scale inset shows a sodium oxide concentration of $\sim 0.2\%$ inside the layer.

or for mass concentrations

$$C_{Na_2O} = 1.02\, C_{Al_2O_3} + 0.09. \quad (8)$$

The above relation could be explained quantitatively by the equality of sodium chemical potential in the substrate and in the thin film, where sodium is both a charge compensator for aluminum and a network modifier following the exchange with protons. Therefore, the different sodium content for the two samples in Fig. 1 is a direct consequence of the presence or absence of aluminum in the layer. The glass composition of the thin films for annealing times greater than 15 minutes is reported in Table 2. Since alkali migration happens fast and reaches a partial equilibrium rapidly for alkali, we can consider that after 15 minutes the interaction between layer and substrate results from the interdiffusion of the substrate and silicate layers of compositions given by Table 2. Compared to our previous paper [1], this contribution focusses on such later interactions and interdiffusion phenomena.

As shown in Fig. 1, a gradual homogenization process sets in between the substrate and the layer. In Fig. 1a)-d) we show the concentration profiles of silicon, aluminum, calcium and sodium oxides in the pure silica layer for increasing duration of the thermal annealing. A consumption process of the silica layer seems to be at play. The interface between the layer and the substrate keeps receding with time as visible for the profiles of silicon, sodium and calcium, which all show an abrupt front gradually moving toward the surface. As a result, the width of the silica layer (as defined by the >95 wt% silica zone in Fig. 1 a) becomes smaller with time. While the distance between front and initial interface after 4 hours is significant, about 60 nm, we note that for these three elements (silicon, sodium and calcium), the width of the fronts did not noticeably grow. In contrast, the evolution of the aluminum is more complex and exhibits an asymmetrical concentration profile. While the presence of an abrupt front can still be identified from the side of the thin film, we observe the superimposition of an interdiffusion process that gradually erodes the abrupt front, as if two different kinetics were simultaneously at play.

Similar trends can be recovered in the evolution upon annealing time of the concentration profiles in the aluminum-doped layer. Silicon, sodium and calcium oxides show here strongly asymmetrical profiles. A steep front can again be identified in the silica-rich part. In comparison with the previous case, we note that the interface shift is faster and that the front is wider. In addition, we observe the interdiffusion between the silica layer and the glass substrate, with an interfacial zone defined by a non-zero gradient of the different species. The width of the interfacial zone becomes larger with time. The advance of the front is thus by an interdiffusion process that expands almost symmetrically on both sides of the initial interface between the film and the substrate. Finally, aluminum shows a rather symmetrical interdiffusion profile.

Table 2: Composition (in weight percent) of the four silica layers after alkali migration.

oxides	pure	0.5%-doped	0.8%-doped	4.3%-doped
SiO_2	99.8 ± 0.2	98.8 ± 0.2	98.3 ± 0.2	91.1 ± 0.2
Na_2O	0.13 ± 0.01	0.66 ± 0.02	0.88 ± 0.03	4.0 ± 0.2
Al_2O_3	0.00 ± 0.00	0.50 ± 0.03	0.77 ± 0.04	4.3 ± 0.2
K_2O	0.007 ± 0.001	0.034 ± 0.001	0.053 ± 0.002	0.25 ± 0.02

3.2. Rate of consumption of silica layer

Comparing the silica profiles in Fig. 1 a) and e) shows that the silica layer (the plateau of high-silica content) recedes much faster with time for the doped layer compared to the pure silica layer. We measure the consumed distance $d(t)$ as the distance between the initial interface and the concentration drop from the high-silica plateau (defined arbitrarily as 95 % of the plateau value). For better accuracy, profilometry on SIMS craters stopped at the two depths (the initial interface and the sharp drop) is carried out to measure the consumed distances. The evolution of the consumed distance with time is plotted in Fig. 2 for three different silica layer compositions: pure silica, 0.5 wt% and 4.3 wt% alumina doping. For each composition, the consumed distance is fitted with a diffusive law:

$$d(t) = \sqrt{D(t - t_0)}. \quad (9)$$

The initial time t_0 corresponds to an induction time before the interdiffusion starts, and it is approximately the same (between 19 and 25 minutes) for the three compositions. The fitted diffusion coefficients D are given in Table 3. The consumption rate increases significantly even for modest alumina doping, since a 4.3 wt% doping multiplies the consumption rate by a factor of 3 compared to the pure silica case.

3.3. Rescaling of concentration profiles

Fig. 2 suggests that independently of the aluminum doping, the consumption of the silica layer is a purely diffusive process, since it scales with $\sqrt{t}$. In order to confirm that diffusion alone can account for the evolution of the chemical profiles, we have plotted in Fig. 3

Table 3: Effective diffusivity for the consumption rate.

Al_2O_3 doping (wt%)	D ($\times 10^{-18} m^2.s^{-1}$)
0	0.3
0.5	0.4
4.3	1.0

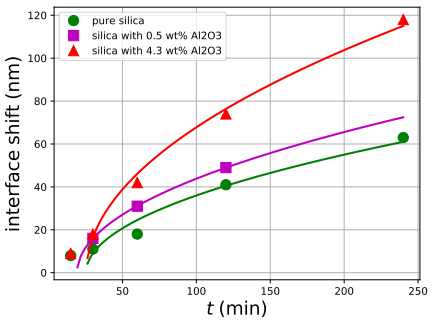

Figure 2: Consumption distance for three types of silica thin films, as a function of annealing durations at 650°C.

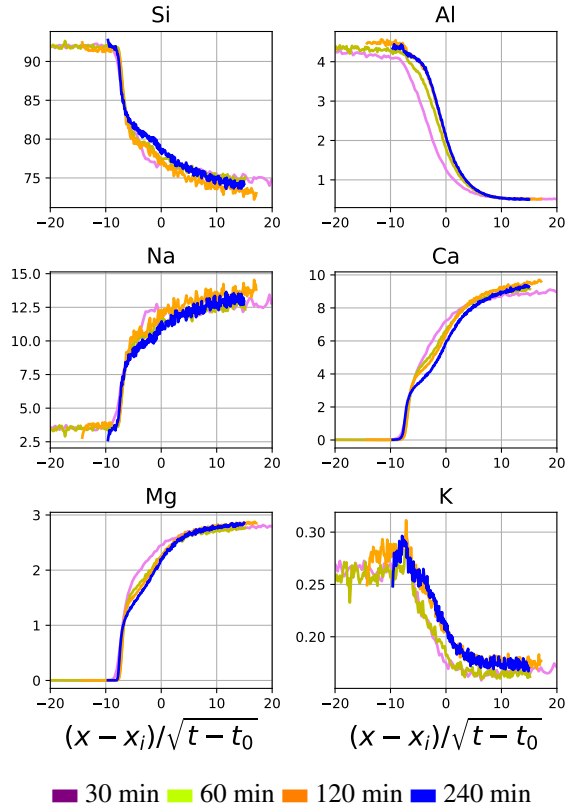

Figure 3: Composition of the different chemical species for the 4.3 wt% doped layer, for times between 30 and 240 minutes at 650°C, represented as a function of rescaled depth $u = \frac{x-x_i}{\sqrt{t-t_0}}$.

the concentration profiles of the different elements as a function of rescaled depth

$$u = \frac{x - x_i}{\sqrt{t - t_0}} \tag{10}$$

where x_i is the position of the initial interface and t_0 is the initial time fitted in Fig. 2. The rescaled profiles at 1, 2 and 4 hours collapse, thus confirming the diffusive nature of the process. The profiles at 30 minutes do not follow exactly the same master curve, probably because of finite-time effects due to incomplete alkali migration.

4. Discussion

Transport properties of silicate glasses such as diffusivity and viscosity are highly dependent on temperature and concentration of network modifier ions. Diffusive transport in the context of the high concentration gradients present at the interface between a float glass substrate and a silica-rich thin film are thus expected to be complex. In the following we discuss first the effect of the rapid sodium uptake on the viscosity and silicon diffusivity of the thin films. We then give a quantitative analysis of our results in the light of a simple model of concentration-dependent diffusivity. Using the framework of multi-component diffusion, we finally identify the elementary exchange mechanisms at play in the interdiffusion process and show that they are consistent with recent results obtained in bulk sodium and calcium aluminosilicate glasses [36].

4.1. Viscosity and glass transition of silicate thin films

Both the consumption rate and the shape of concentration profiles are very different for the pure silica and the doped silica layers (Figs. 1 and 2). Qualitatively, this difference can be explained by a large difference of silicon diffusivity between the two kinds of thin films, due to the larger alkali content in the doped layer. A first estimation of this difference of diffusivity can be obtained from the difference of viscosity between the two regions, viscosity scaling as the inverse of silicon diffusivity according to Eyring's law. In order to estimate the viscosity of the different thin film and substrate compositions, we have used the model of Priven [37]. We do not expect a high accuracy of the model for thin films compositions, since our compositions lie outside of domains for which experimental viscosity measurements have been performed in the sodium aluminosilicate system [38, 39]. Nevertheless, the model of Priven is useful to understand the variations of viscosity with aluminum (and hence sodium) content. In Fig. 4 we have plotted the viscosity at 650°C

(Fig. 4 a)) and the glass transition temperature (Fig. 4 b)) of silica layers with an increasing aluminum content, and a sodium content proportional to the aluminum content as in Eq. (7). The viscosity decreases rapidly as more aluminum and sodium is incorporated in the thin film. Aluminum and charge-compensating sodium ions should not decrease the viscosity [39], since they do not lead to the depolymerization of the network. However, sodium ions present as network modifiers depolymerize the aluminosilicate network, and we have shown [1] that their quantity is proportional to the aluminum content.

Interestingly, the viscosity of the doped layer (with 4.3 wt% Al_2O_3) at 650°C is slightly above 10^{12} Pa.s, which is the viscosity at the glass transition. Therefore, after alkali migration, the viscosity of the doped layer is compatible with structural rearrangements and diffusion of all species, including network formers, inside the layer. On the other hand, the viscosity of the pure or $0.5-0.8$ wt% Al_2O_3 layers is much higher (see Fig. 4), and their glass transition temperatures (between 820°C and 760°C) are far above the annealing temperature (nevertheless, glass transition temperatures after alkali migrations are all much lower than glass transition temperatures of aluminosilicate compositions without alkali, of the order of 1200°C). Therefore, for the pure or 0.5-0.8 wt% Al_2O_3 layers, diffusion of network formers is possible only at the interface between the layer and less polymerized compositions. Note that our estimations of viscosity and glass transition are consistent with the experiments of Le Losq et al. [40] in sodium aluminosilicate supercooled liquids.

4.2. Interdiffusion in the presence of diffusivity gradient

Fig. 4 also indicates the viscosity η at 650°C of the substrate, which is of the order of 10^9 Pa.s. For all layer compositions, there is a viscosity contrast of several orders of magnitude between the layer and the substrate. The viscosity contrast is more pronounced for low aluminum and sodium content. Across the composition profile, the viscosity gradient translates into a diffusivity gradient for silicon, because of the Eyring relation between diffusivity D and viscosity η

$$D = \frac{k_B T}{\eta d}, \tag{11}$$

where k_B is the Boltzmann constant, T the temperature, and d a typical jump distance for diffusion. In this subsection, we model the silica profiles of Fig. 1 using a concentration-dependent model for silica diffusivity.

Since the diffusivity of silicon scales as the inverse of viscosity [25], and the logarithm of the viscosity empirically varies linearly with concentrations [41], we expect

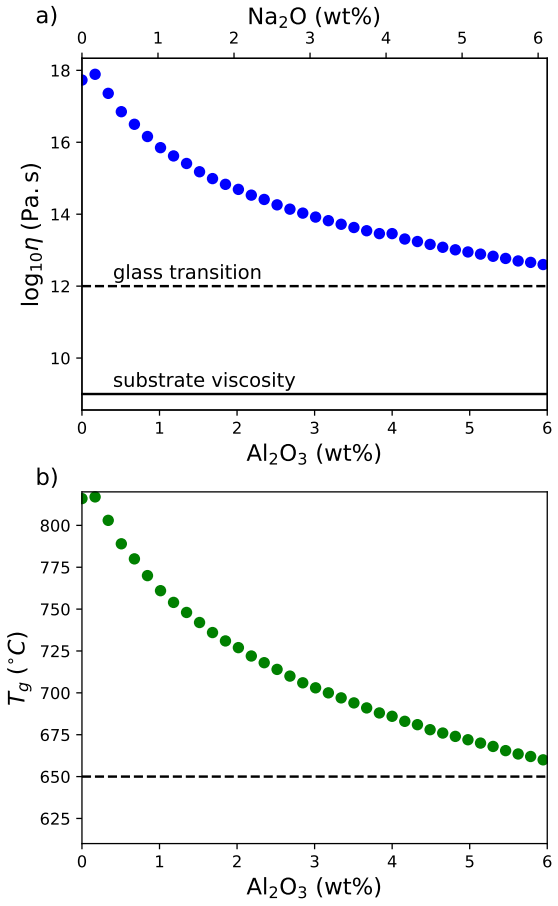

Figure 4: (a) Viscosity of silica layers at 650°C as a function of Al_2O_3 doping content. The corresponding Na_2O content after the fast alkali migration is indicated as upper ticks. Substrate viscosity is indicated with a solid line, while the viscosity of supercooled liquids at their glass transition is indicated with a dashed line. (b) Glass transition temperature (T_g) as a function of Al_2O_3 doping content. The annealing temperature 650°C is shown with a dotted line.

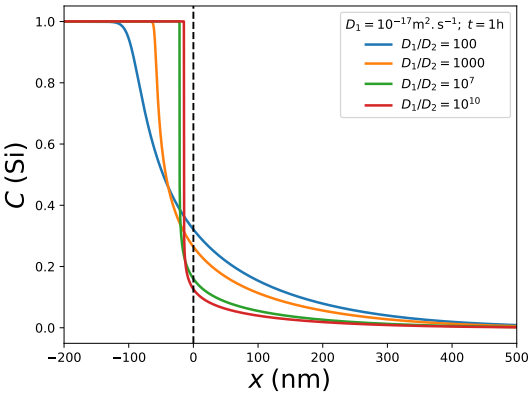

Figure 5: Theoretical concentration profiles for a diffusivity coefficient with an exponential dependence on concentration. Different profiles correspond to the same diffusion time and diffusivity of the "substrate" (right part), but to different diffusivity ratios ranging from 100 to 10^{10} between the two regions initially put in contact.

the diffusivity of silicon to decrease exponentially with silicon concentration:

$$D_{\mathrm{Si}} = D_0 \exp(-\beta C_{\mathrm{Si}}). \tag{12}$$

In the above expression, β encodes the strength of the dependence on concentration. For two different liquids put in contact at $t = 0$, with respective concentrations C_1 and C_2 and respective diffusivities D_1 and D_2, we have

$$\beta = \frac{1}{C_2 - C_1} \log\left(\frac{D_1}{D_2}\right). \tag{13}$$

Crank [42] proposed an elegant way to solve the diffusion equation in an infinite medium, for a diffusivity given by Eq. (12). The resolution is based on a change of coordinates, so that an ordinary differential equation is solved instead of a partial difference equation. We implemented the resolution using the Python library `scipy`.

Fig. 5 shows theoretical normalized concentration profiles ($C_1 = 0$, $C_2 = 1$) for the same diffusion time (1h) and value of D_1 ($D_1 = 10^{-17} m^2.s^{-1}$ from [36]) in the less viscous substrate, and for ratios of diffusivities (linked to β by Eq. (13)) ranging from 10^2 to 10^{10}. As the ratio of diffusivities increases, the concentration profile becomes more and more asymmetric, with a steeper and steeper interface on the more viscous side. Also, the diffusion width decreases on both sides of the initial interface when D_2 decreases. We observe that profiles corresponding to the low ratios of diffusivities (100 and 1000) look similar to silica profiles for the doped layer (Fig. 1 e), with an asymmetric but smooth diffusion profile. On the other hand, for the largest diffusivity ratios, concentration profiles resemble the silica profiles for the pure-silica layer (Fig. 1 a).

To go beyond this qualitative agreement, we fitted the silica profile of Fig. 1 e) (4.3 wt% Al_2O_3, $t = 2h$) with the model of Eq. (12). The best fit is shown in Fig. 6, corresponding to estimated parameters $D_1/D_2 = 1.1\times10^3$ and $D_1 = 8.10^{-18}$ m^2.s^{-1}. The diffusivity ratio is consistent with the viscosity ratio of Fig. 4, which is estimated to be 1000 for the 4.3 wt% doped layer. As for the diffusion of silicon in the glass substrate, Claireaux et al. [36] measured a diffusivity of 10^{-17} m^2.s^{-1} at 650°C, for a sodium and calcium aluminosilicate composition. Therefore, the fitted coefficients (reported in Table 4) are consistent with existing literature data, and Eq. (12) provides a way to estimate the viscosity of the thin films.

For the silica layer doped with 0.8 wt%, for which the annealing temperature of 650°C is well below its glass transition, the fitted substrate diffusivity is similar to the one found with the 4.3 wt% layer ($D_1 = 7.10^{-18}$ m^2.s^{-1}). We estimate a diffusivity ratio of 4.10^5, which is slightly smaller than the estimated ratio of viscosities 10^6. Given the fact that, below the glass transition, our viscosity model is not accurate and the validity of the Eyring relation is not certain, the agreement with literature values is very reasonable. We did not attempt to fit the diffusivity ratio for the pure silica layer, since the silica profile is too steep for a correct fit.

The estimated values of diffusivities of silicon in substrate and layer are given in Table 4. Note that consumption rates of layers given in Table 3 lie in between the diffusivities of silicon in substrate and layer. However, the consumption rate is closer to the value in the substrate.

Alumina profiles (Fig.1 b) and f)) are more symmetric than silica profiles, and less extended inside the substrate. If we apply the same fitting procedure to the alumina profiles for the different layers, we find different values than for silica profiles both for the diffusion coefficient of aluminum in the substrate ($D_1 = 10^{-19}$ m^2.s^{-1}) and for the diffusivity ratio $D_1/D_2 = 4$. Therefore, aluminum diffuses more slowly than silicon. Since the aluminum diffusion distance is smaller than the consumed width of the layer, the aluminum gradient is found in a region where the silicon profile is smooth. This might explain why the aluminum profile is more symmetric.

4.3. Multidiffusion and coupled exchanges

In this section we focus on the silica layer doped with 4.3 wt% Al_2O_3, since its diffusion profiles are smoother and hence easier to interpret. We have seen that the two

Table 4: Estimation of silicon diffusivities

	D_1 (substrate)	D_2 (layer)	D_1/D_2	viscosity ratio
0.8% Al_2O_3	7.10^{-18} $m^2.s^{-1}$	$1.5.10^{-22}$ $m^2.s^{-1}$	4.10^5	10^6
4.3% Al_2O_3	8.10^{-18} $m^2.s^{-1}$	7.10^{-21} $m^2.s^{-1}$	1100	1000

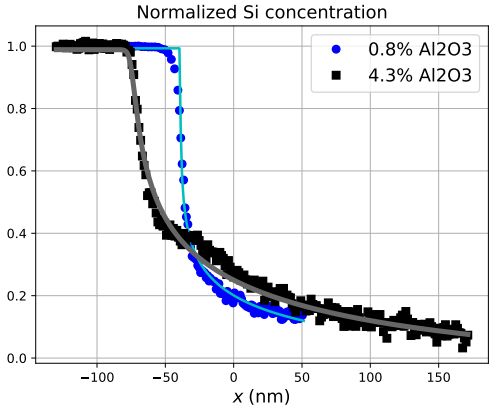

(a)

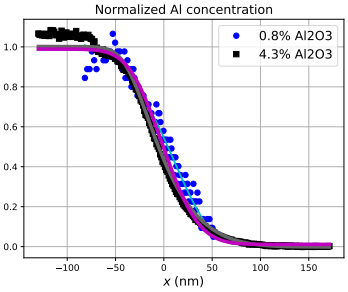

(b)

Figure 6: (a) Normalized silicon profiles after two hours of annealing at 650°C, for silica layers doped with 0.8 wt% and 4.3 wt% of Al_2O_3. Solid lines represent the best least-square fits of experimental data with a concentration-dependent diffusivity (Eq. (12)). (b) Aluminum profiles after two hours of annealing at 650°C, for silica layers doped with 0.8 wt% and 4.3 wt% of Al_2O_3. Solid lines represent the best least-square fits of experimental data with a concentration-dependent diffusivity (Eq. (12)).

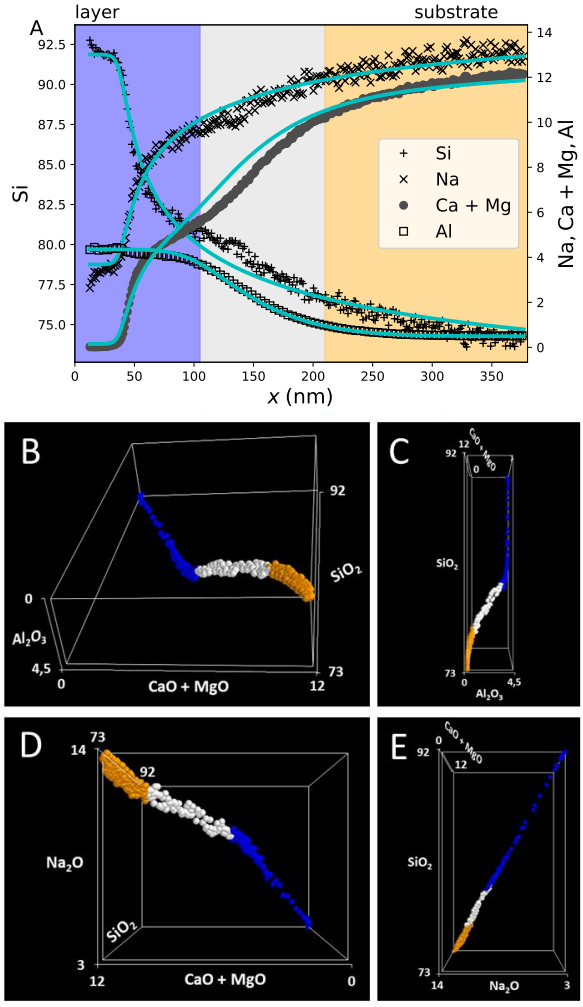

Figure 7: A-Compositions profiles of Fig. 1 (left column) for the 4.3 wt% doped layer after 4 hours at 650°C, reproduced here to show the three regions represented in different colors in composition trajectories. Symbols correspond to measurements, and solid lines to least-square fits of multicomponent diffusion. B-E Composition trajectories for the profiles of A, for different angles of view and Na_2O (resp. Al_2O_3) as dependent component in B-C (resp. D-E). Colors correspond to the three zones in A.

network formers diffuse with different rates. Moreover, the profiles of network modifiers seem to depend on the ones of network formers, with sodium (see Fig. 3) being the inverted profile of silicon, while calcium and magnesium seem to counter-diffuse with aluminum close to the initial interface, and with silicon at further distance. The two alkali-earth species profiles display an inflexion because of the superimposition of the two mechanisms. Such couplings between species are well accounted for by the *diffusion matrix* formalism [26]. In this section we try to obtain a quantitative description of couplings between species.

The diffusion matrix links the flux of one element to the gradients of all species. Eigenvectors of the diffusion matrix can be interpreted as elementary exchange reactions, while the corresponding eigenvalues represent the interdiffusion coefficients of such exchanges. In order to determine the coefficients of the diffusion matrix, several diffusion experiments are needed, corresponding to concentration gradients along different directions in composition space. Here we only have one direction with the exchange of silica and glass substrate (even if we have both pure and doped silica layers, the direction of the exchanges are almost collinear), so that it is not possible to determine the full diffusion matrix. Nevertheless, it is possible to use information from literature about the direction of exchanges.

Diffusion matrix of sodium and calcium aluminosilicate system -. Claireaux et al. [36] have recently determined the diffusion matrix in a sodium and calcium aluminosilicate composition at 650°C. The authors obtained the following eigenvectors (exchange reactions) and their corresponding diffusion rates:

$$\mathrm{Na_2O} \leftrightarrow \mathrm{CaO} \quad \alpha_1 = 2.10^{-15}\mathrm{m^2.s^{-1}} \tag{14}$$

$$\mathrm{CaO} \leftrightarrow \mathrm{SiO_2} \quad \alpha_2 = 2.10^{-17}\mathrm{m^2.s^{-1}} \tag{15}$$

$$\mathrm{CaO} \leftrightarrow \mathrm{Al_2O_3} \quad \alpha_3 = 7.10^{-19}\mathrm{m^2.s^{-1}}. \tag{16}$$

The first exchange can also be written as the exchange of network modifiers $2\mathrm{Na^+} \leftrightarrow \mathrm{Ca^{2+}}$, while the other ones involve both network-forming cations and oxygen, and are therefore slower. If we suppose that magnesium plays the same role as calcium, the initial concentration difference between substrate and layer after alkali migration can be decomposed in the above basis of eigenvectors

$$\mathbf{\Delta C} = \mathbf{C}_{\mathrm{substrate}} - \mathbf{C}_{\mathrm{layer}} = \begin{pmatrix} 10\% \\ 20\% \\ 4\% \end{pmatrix} \begin{matrix} \mathrm{Na_2O} \leftrightarrow \mathrm{CaO} \\ \mathrm{CaO} \leftrightarrow \mathrm{SiO_2} \\ \mathrm{CaO} \leftrightarrow \mathrm{Al_2O_3} \end{matrix} . \tag{17}$$

However, a macroscopic exchange of sodium and calcium, corresponding to the first eigenvector, is not possible since only a negligible amount of calcium is present in the thin film. Therefore, the diffusion of sodium is controlled by the amount of calcium from the substrate which exchanges with silicon from the film, that is, by the dynamics of the second exchange. The resulting reaction is the sum of the two eigenvectors, weighted by their coefficient (Eq. (17)):

$$0.1\mathrm{Na_2O} + 0.1\mathrm{CaO} \leftrightarrow 0.2\mathrm{SiO_2} \tag{18}$$

or

$$\frac{1}{2}\mathrm{Na_2O} + \frac{1}{2}\mathrm{CaO} \leftrightarrow \mathrm{SiO_2}. \tag{19}$$

In order to verify that the diffusion matrix of [36] can be applied to our experiments, we fit experimental profiles using the exchange reactions of Eqs. (19) and (16). The diffusion matrix of [36] was measured for a narrow composition region, in which diffusion coefficients are constant. In order to account for the strong compositions gradients of our experiments, we need to introduce a composition dependence for each diffusion eigenvalue, of the form of Eq. (12). Fig. 7 (a) shows the diffusion profiles of $\mathrm{SiO_2}$, $\mathrm{Al_2O_3}$, $\mathrm{Na_2O}$ and CaO + MgO after 4 hours, and the best-fit theoretical diffusion profiles. The agreement between experimental profiles and fits is good. Therefore, measured concentration profiles are consistent with the diffusion matrix of [36], with the only difference that it has been necessary to introduce a concentration-dependence of the diffusion rate implying silicon. Diffusion exchanges with thin films of different compositions in the sodium and calcium aluminosilicate space could therefore be predicted using the eigenvectors of [36] and the concentration-dependent diffusivity of Eq. (12), with the following coefficients:

$$\mathrm{Na_2O} \leftrightarrow \mathrm{CaO} \quad D_1 = 7^{-18}\mathrm{m^2.s^{-1}} \quad D_2 = 1.10^{-20}\mathrm{m^2.s^{-1}} \tag{20}$$

$$\mathrm{CaO} \leftrightarrow \mathrm{SiO_2} \quad D_1 = 7.10^{-18}\mathrm{m^2.s^{-1}} \quad D_2 = 1.10^{-20}\mathrm{m^2.s^{-1}} \tag{21}$$

$$\mathrm{CaO} \leftrightarrow \mathrm{Al_2O_3} \quad D_1 = 1.10^{-19}\mathrm{m^2.s^{-1}} \quad D_2 = 2.10^{-20}\mathrm{m^2.s^{-1}} \tag{22}$$

One should note that diffusion data were obtained here at 650°C for annealing times of a few hours, while the experiments of [36] lasted for 40 days. This was made possible by the excellent resolution of SIMS profilometry (as compared with electron microprobe analysis), but it comes at the cost of a difficult calibration of SIMS signal [1]. It has been suggested by other authors [43] that the thin film on substrate configuration was an interesting technique to obtain kinetic data of silicate materials, when combined with appropriate microanalysis techniques.

For a complete description of multidiffusion, one should add the fastest eigenvector, that is the $Na^+ \leftrightarrow H^+$ exchange evidenced in [1]. However, the corresponding diffusivity coefficient is much faster than the ones of other eigenvectors, and experiments at lower temperature or with a thicker silica film would be needed in order to determine it.

Diffusion paths in composition space: a graphical representation of couplings. In order to visualize multicomponent couplings, one can plot diffusion paths in concentration space [26, 34]. Since the number of oxides is too large for visualization of the composition space, we only consider the major oxides, and we consider together the two alkali-earth species, so that we are left with four dimensions: SiO_2, Al_2O_3, Na_2O, $CaO + MgO$. Because of mass conservation, the sum of the coefficients corresponding to these four dimensions is constant, so that it is possible to represent a composition point in a 3-dimensional space, like in Fig. 7 B-E. In Fig. 7 B-C, compositions are plotted in the (SiO_2, Al_2O_3, $CaO + MgO$) space, Na_2O being the dependent species. In Fig. 7 D-E, Al_2O_3 is the dependent species. For an easier visualization, we have divided the profile into three zones, with white points corresponding to the zone where aluminum has diffused significantly, and blue (resp. orange) on the left (closer to the surface) and right (deeper into the substrate) of this central zone (see Fig. 7 A for the boundaries of these zones). For the 3-D plot in composition space, we have excluded the points closest to the surface because of SIMS artefacts.

Fig. 7 B shows that the diffusion trajectory is not a straight line, which confirms the presence of multicomponent effects. Blue points lie on a straight line corresponding to the exchange of silicon with alkali and alkali-earth species, that is to the exchange of Eq. (19). No aluminum is involved in this exchange (as shown for example in Fig. 7 C), since the eigenvalue of Eq. (16) is much smaller, so that the latter exchange does not contribute to the diffusion path far from the initial interface. The orange part has a direction comparable to the blue one, but this part of the diffusion trajectory is less straight. A linear regression of the points of the blue zone, in order to obtain the equation of the straight line, confirms the stoechiometry of the dominant exchange:

$$0.90SiO_2 + 0.04Al_2O_3 \leftrightarrow 0.51Na_2O + 0.43(CaO + MgO), \quad (23)$$

meaning that silicon is exchanged with alkali and alkali-earth ions in equal proportions, consistently with Eq. (19) and [36]. If we apply the same procedure to the orange zone, deep inside the substrate, we obtain a comparable equation

$$0.84SiO_2 + 0.11Al_2O_3 \leftrightarrow 0.43Na_2O + 0.51(CaO + MgO). \quad (24)$$

The white zone, close to the initial interface is the only region where the effect of exchange (16) is significant. Fig. 7 C shows that the white zone is the only one where the concentration of aluminum changes. In this region, the composition path is a linear combination of both exchanges (19) and (16), involving respectively silicon and aluminum.

5. Conclusions

In this work and in its previous companion paper [1], we have evidenced several diffusion phenomena at play during the interaction between Al:doped silica layers and soda-lime glass substrate, at 650°C:

- A rapid migration of sodium (and potassium to a lesser extent) from the substrate to the layer, counter-diffusing with protons from the layer [1]. The corresponding diffusion coefficient is fast enough ($D > 10^{-17}\,m^2.s^{-1}$) so that a partial equilibrium concentration of sodium oxide in the layer is reached in a few minutes, corresponding to 1.5× the molar concentration of Al_2O_3.
- The diffusion of silicon, present in excess in the thin film, counter-diffusing with sodium, calcium and magnesium which are in excess in the substrate. The rate of this exchange is controlled mainly by the diffusivity of silicon in the super-cooled substrate, but also by the slower diffusivity of silicon in the layer. The latter diffusivity depends strongly on the alkali content of the layer, with alkali ions decreasing the viscosity of the layer and increasing the mobility of silicon. Hence, the larger the aluminum doping, the faster the diffusivity of silicon and the consumption rate of the layer. The equivalent diffusivity describing the shift of the layer interface was found to be between $0.3.10^{-18} m^2.s^{-1}$ (for a pure silica layer) and $10^{-18} m^2.s^{-1}$ (for a 4.3 wt% Al_2O_3-doped layer).
- In the case of Al:doped layers, the diffusion of aluminum, counter-diffusing with alkali-earth species from the substrate. This exchange is significantly slower than the one involving silicon, with a diffusion rate of $10^{-19} m^2.s^{-1}$.

In addition to the characterization of these different mechanisms and their kinetics, we have developed a

methodology to process complex diffusion profiles with a concentration-dependent diffusivity and multicomponent couplings, which makes it possible to estimate local diffusion coefficients both in layer and substrate.

Future work will extend this methodology to other substrate compositions of industrial interest (such as borosilicate compositions) and silica layers doping elements such as boron or zinc.

Acknowledgments

The authors gratefully acknowledge Thierry Crétin, Corinne Papret and Régine Faure for SIMS measurements at Saint-Gobain Recherche in Aubervilliers (France), as well as Franck Pigeonneau for help in solving Crank's model. The authors also acknowledge the experimental help of Raphaël Danguillaume, Anne Lelarge, Benoît Louis and Jean-Paul Rousseau, as well as enlightening discussions with Corinne Claireaux and Mike Toplis.

References

[1] Fonné JT, Burov E, Gouillart E, Grachev S, Montigaud H, Vandembroucq D. Aluminum-enhanced alkali diffusion from float glass to PVD-sputtered silica thin films. Journal of the American Ceramic Society. 2018;101(4):1516–1525.

[2] Schaefer C, Bräuer G, Szczyrbowski J. Low emissivity coatings on architectural glass. Surface and Coatings Technology. 1997;93(1):37–45.

[3] Selvakumar N, Barshilia HC. Review of physical vapor deposited (PVD) spectrally selective coatings for mid-and high-temperature solar thermal applications. Solar Energy Materials and Solar Cells. 2012;98:1–23.

[4] Raut HK, Ganesh VA, Nair AS, Ramakrishna S. Anti-reflective coatings: A critical, in-depth review. Energy & Environmental Science. 2011;4(10):3779–3804.

[5] Janke N, Graßme O, Weißmann R. Alkali ion migration control from flat glass substrates. Glass Science and Technology. 2000;73:143–155.

[6] Scofield JH, Asher S, Albin D, Tuttle J, Contreras M, Niles D, et al. Sodium diffusion, selenization, and microstructural effects associated with various molybdenum back contact layers for CIS-based solar cells. In: 24th IEEE Photovoltaic Specialists Conference. vol. 1;. p. 164–167.

[7] Durose K, Cousins MA, Boyle DS, Beier J, Bonnet D. Grain boundaries and impurities in CdTe/CdS solar cells. Thin Solid Films. 2002;403-404:396–404.

[8] Emziane M, Durose K, Halliday DP, Romeo N, Bosio A. The distribution of impurities in the interfaces and window layers of thin-film solar cells. Journal of Applied Physics. 2005;97(11):114910.

[9] Lee JM, Choi BH, Ji MJ, An YT, Park JH, Kwon JH, et al. Effect of barrier layers on the properties of indium tin oxide thin films on soda lime glass substrates. Thin Solid Films. 2009;517:4074–4077.

[10] Kulczyk-Malecka J, Kelly PJ, West G, Clarke GCB, Ridealgh JA. Investigations of diffusion behaviour in Al-doped zinc oxide and zinc stannate coatings. Thin Solid Films. 2011;520(5):1368–1374.

[11] Kulczyk-Malecka J, Kelly PJ, West G, G C B C, Ridealgh JA. Diffusion studies in magnetron sputter deposited silicon nitride films. Surface and Coatings Technology. 2014;255:37–42.

[12] Heft A, Tölke T, Pfuch A, Erbe C. Photocatalytically active thin films on float glass with enhanced hydrophilicity and transmission for photovoltaic applications. Solar energy materials and solar cells. 2006;90(17):2846–2854.

[13] Ghazzal MN, Aubry E, Chaoui N, Robert D. Effect of SiN_x diffusion barrier thickness on the structural properties and photocatalytic activity of TiO_2 films obtained by sol-gel dip coating and reactive magnetron sputtering. Beilstein J Nanotechnol. 2015;6:2039–45.

[14] Fehlner FP, Binkowski NJ, Salisbury KR, Button L. Alumina barrier layers on LCD glass. Journal of Non-Crystalline Solids. 1996;195:89–94.

[15] Fehlner FP. Thin films on glass for liquid crystal displays. Journal of Non-Crystalline Solids. 1997;218:360–367.

[16] Wolfe JD, Boehmler C, Hofmann JJ. Method for coating substrates with silicon based compounds - EP0502068B1 [Patent]. Google Patents; 1995.

[17] Pretorius R, Harris J, Nicolet M. Reaction of thin metal films with SiO_2 substrates. Solid-State Electronics. 1978;21(4):667–675.

[18] Ono H, Katsumata T. Interfacial reactions between thin rare-earth-metal oxide films and Si substrates. Applied Physics Letters. 2001;78(13):1832–1834.

[19] Cho M, Park J, Park HB, Hwang CS, Jeong J, Hyun KS. Chemical interaction between atomic-layer-deposited HfO_2 thin films and the Si substrate. Applied physics letters. 2002;81(2):334–336.

[20] Wu BC, Chang E, Chang SF, Tu D. Degradation Mechanisms of ZrO_2–8 wt% Y_2O_3/Ni–22 Cr–10 Al–1 Y Thermal Barrier Coatings. Journal of the American Ceramic Society. 1989;72(2):212–218.

[21] Wang X, Zhu S, Li Z, Zhang Y, Chen M, Wang F. Interfacial microstructure evolution of glass-based coating on IC10 superalloy with a Ni_3Al bond-coat at 1050°C. Journal of the American Ceramic Society. 2017;100(8):3451–3466.

[22] Freer R. Diffusion in silicate minerals and glasses: a data digest and guide to the literature. Contributions to Mineralogy and Petrology. 1981;76(4):440–454.

[23] Chakraborty S. Diffusion in silicate melts. Reviews in Mineralogy and Geochemistry. 1995;32(1):411–503.

[24] Zhang Y, Ni H, Chen Y. Diffusion data in silicate melts. Reviews in Mineralogy and Geochemistry. 2010;72(1):311–408.

[25] Mungall JE. Empirical models relating viscosity and tracer diffusion in magmatic silicate melts. Geochimica et Cosmochimica Acta. 2002;66(1):125–143.

[26] Liang Y. Multicomponent diffusion in molten silicates: theory, experiments, and geological applications. Reviews in Mineralogy and Geochemistry. 2010;72(1):409–446.

[27] Varshneya A, Cooper A. Diffusion in the System K_2O–SrO–SiO_2: III, Interdiffusion Coefficients. Journal of the American Ceramic Society. 1972;55(6):312–317.

[28] Sugawara H, Nagata K, Goto K. Interdiffusivities matrix of CaO–Al_2O_3–SiO_2 melt at 1723°K to 1823°K. Metallurgical Transactions B. 1977;8(3):605–612.

[29] Kress V, Ghiorso M. Multicomponent diffusion in MgO–Al_2O_3–SiO_2 and CaO–MgO–Al_2O_3–SiO_2 melts. Geochimica et Cosmochimica Acta. 1993;57(18):4453–4466.

[30] Trial AF, Spera FJ. Measuring the multicomponent diffusion matrix: Experimental design and data analysis for silicate melts. Geochimica et Cosmochimica Acta. 1994;58(18):3769–3783.

[31] Liang Y, Richter FM, Watson EB. Diffusion in silicate melts: II. Multicomponent diffusion in CaO–Al_2O_3–SiO_2 at 1500°C and

1 GPa. Geochimica et Cosmochimica Acta. 1996;60(24):5021–5035.

[32] Mungall JE, Romano C, Dingwell DB. Multicomponent diffusion in the molten system K_2O-Na_2O-Al_2O_3-SiO_2-H_2O. American Mineralogist. 1998;83:685–699.

[33] Richter FM, Liang Y, Minarik WG. Multicomponent diffusion and convection in molten MgO-Al_2O_3-SiO_2. Geochimica et Cosmochimica Acta. 1998;62(11):1985–1991.

[34] Claireaux C, Chopinet MH, Burov E, Gouillart E, Roskosz M, Toplis MJ. Atomic mobility in calcium and sodium aluminosilicate melts at 1200°C. Geochimica et Cosmochimica Acta. 2016;192:235–247.

[35] Chakraborty S, Dingwell DB, Rubie DC. Multicomponent diffusion in ternary silicate melts in the system K_2O-Al_2O_3-SiO_2: II. Mechanisms, systematics, and geological applications. Geochimica et Cosmochimica Acta. 1995;59(2):265–277.

[36] Claireaux C, Chopinet MH, Burov E, Gouillart E, Roskosz M, Toplis MJ. Influence of temperature on multicomponent diffusion in calcium and sodium aluminosilicate melts. Journal of Non-Crystalline Solids (accepted). 2018;.

[37] Priven AI. General Method for Calculating the Properties of Oxide Glasses and Glass-Forming Melts from their Composition and Temperature. Glass Technology. 2004;45(6):244–254.

[38] Toplis MJ, Dingwell DB, Lenci T. Peraluminous viscosity maxima in Na_2O-Al_2O_3-SiO_2 liquids: The role of triclusters in tectosilicate melts. Geochimica et Cosmochimica Acta. 1997;61(13):2605–2612.

[39] Toplis MJ, Dingwell DB, Hess KU, Lenci T. Viscosity, fragility, and configurational entropy of melts along the join SiO_2-$NaAlSiO_4$. American Mineralogist. 1997;82(9-10):979–990.

[40] Le Losq C, Neuville DR, Florian P, Henderson GS, Massiot D. The role of Al^{3+} on rheology and structural changes in sodium silicate and aluminosilicate glasses and melts. Geochimica et Cosmochimica Acta. 2014;126:495–517.

[41] Giordano D, Russell JK, Dingwell DB. Viscosity of magmatic liquids: a model. Earth and Planetary Science Letters. 2008;271(1):123–134.

[42] Crank J. The mathematics of diffusion. Oxford university press; 1979.

[43] Dohmen R, Becker HW, Meißner E, Etzel T, Chakraborty S. Production of silicate thin films using pulsed laser deposition (PLD) and applications to studies in mineral kinetics. European journal of mineralogy. 2002;14(6):1155–1168.